Electronic Supplementary Material (ESI) for RSC Advances.
This journal is © The Royal Society of Chemistry 2017

Metal doped mesoporous FeOOH nanorods for high performance supercapacitor

Rasmita Barik, Bikash Ku. Jena, Mamata Mohapatra*

Hydro and Electrometallurgy Department, CSIR-Institute of Minerals and Materials technology, Bhubaneswar, India, pin-751013, Email- mamatamohapatra@yahoo.com

Raman study

The Raman spectra for the synthesized samples are shown in S1. In case of C1and C2 samples showed different peaks at 232, 297, 395, 470, 550, 597, 632 cm^{-1}, which correspond to Raman bands for different bonding frequencies of goethite. The first four Raman bands are attributed to the A1g mode of Fe–O symmetric stretching, Eg Fe–OH symmetric bending, Eg Fe–O–Fe/–OH symmetric stretching and A1g Fe–OH asymmetric stretching[1]. The Raman bands appearing around 550, 632 cm^{-1} are related to Fe–OH asymmetric stretching and Fe–O symmetric stretching of the goethite phase. Overall shifting in wavenumber has a good relationship with the metal substitution for Fe in the structure of goethite. A1g mode of Fe–O symmetric stretching is shifted to lower wave length as reported for pure goethite. The radius of Co^{2+} (0.77 Å) is slightly more than that of Fe^{3+} (0.65 Å). Therefore, the occurrence of Co-O replacing of Fe-O necessarily increases the bonding length resulting in the decrease of bonding force, which causes the shift of these bands to lower wavenumbers.

Raman band at 660–690 cm^{-1} for solid solutions $FexCr_2–xO_3$[2] was reported. This mode is not group theoretically allowed in Raman spectra and has not been reported for the end-member. However, this could appear due to a strong resonance on the surface arising in the defects structure induced by stress[3]. Generally red shifts (lower wave number) in Raman spectrum are due to residual stress, disorder and crystal defects present in the sample. Another reason could be the existence of surface tension[4].

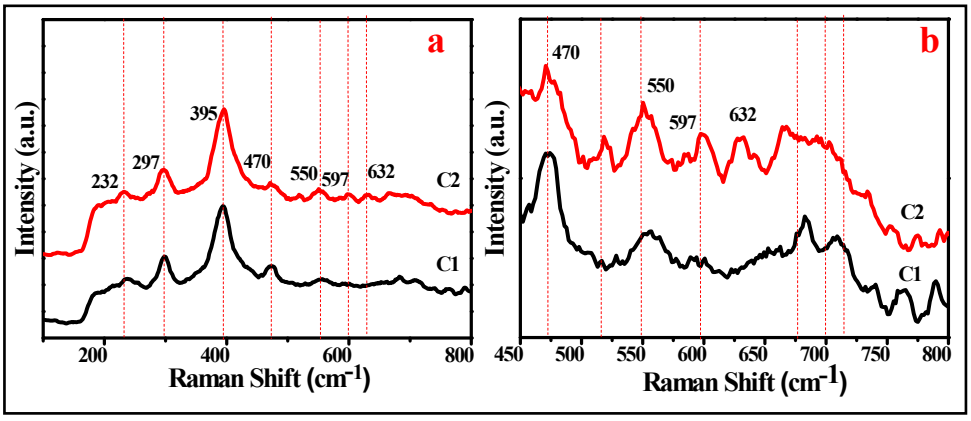

Figure S1. Raman bands (200-800 cm^{-1}) for as synthesized iron oxides **(a, b)** in presence of Co.

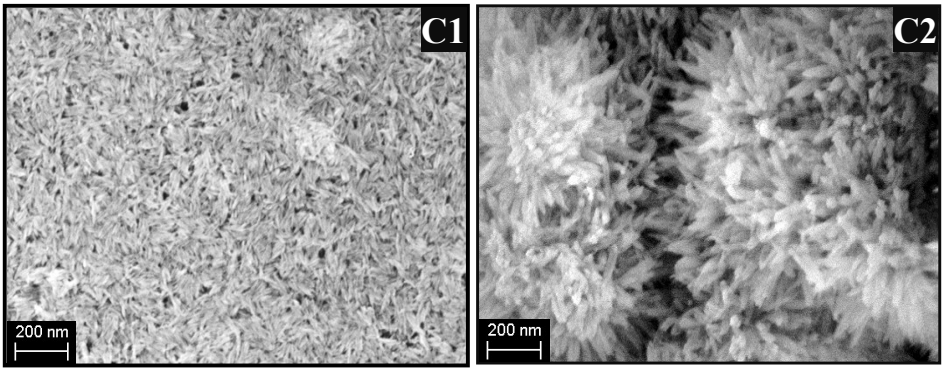

Figure S2. FESEM images of Co doped iron oxides.

Table. S1

Average size of as synthesized goethite particles in presence of Co and Mn, in EG medium (Measured from FESEM observations).

Sample name	L: length (nm)	W: width (nm)	L/W ratio
C1	43.7-50	6.2-12.5	4-7
C2	99. 9-133.2	33.3-53.28	2.5

Table.S2:

Electrode material	Synthesis method	Sp. Capacitance ($F\ g^{-1}$)	Electrolyte	Ref
α-FeOOH	Co-precipitation	160	1M Na_2SO_4	5
rGO based α-FeOOH	Co-precipitation	452	1M KCl	6
FeOOH@PPy electrode	Hydrothermal	1140	2M KOH	7
Reduced graphite oxide (RGO +FeOOH)	----	165.5	1M Na_2SO_3	8
FeO_x/MWNT electrodes	Hydrothermal	300	1M Na_2SO_3	9
FeOOH	Co-precipitation	1110 mF cm^{-2}	3 M KOH	10
$CoFe_2O_4$/FeOOH composites	Hydrothermal	332.4	6 M KOH	11
FeOOH nanorods/graphene oxide (GO)	Hydrothermal	127	1 M KOH	12
Cobalt doped α-FeOOH	Co-precipitation	463.18	1M KOH	Present study

Reference:

1. J. G. Hockridge, F. Jones, M. Loan, W. R. Richmond, **An electron microscopy study of the crystal growth of schwertmannite needles through oriented aggregation of goethite nanocrystals**, J. Cryst. Growth, 311 (2009), pp. 3876-3882.
2. P. C. Rieke, B. D. Marsh, L. L. Wood, B. J. Tarasevich, J. Liu, L. Song, G. E. Fryxell, **Aqueous solution deposition kinetics of iron oxyhydroxide on sulfonic acid terminated self-assembled monolayers,** Langmuir, (11) 1995, pp. 318-326.
3. R. M. Cornell, R. Giovanoli, **Effect of Manganese on the Transformation of Ferrihydrite into Goethite and Jacobsite in Alkaline Media,** Clays and Clay Minerals, 35 (1987), pp. 11-20.
4. H. C. Choi, Y. M. Jung, S. B. Kim, **Size effects in the Raman spectra of TiO_2 nanoparticles,** Vibrational Spectrosc., (37) 2005, pp. 33-38.
5. R. Barik, B. K. Jena, A. Dash, M. Mohapatra, **In situ synthesis of flowery-shaped α-FeOOH/Fe_2O_3 nanoparticles and their phase dependent supercapacitive behaviour**, RSC Adv., 4(2014), pp. 18827–18834.
6. H. Xu, Z. Hu, A. Lu, Y. Hu, L. Li, Y. Yang, Z. Zhang, H. Wu, **Synthesis and super capacitance of goethite/reduced graphene oxide for supercapacitors**, Materials Chemistry and Physics, 141 (2013), pp. 310-317.
7. G. Wei, K. Du, X. Zhao, C. Li, J. Li, K.i Ren, Y. Huang, H. Wang, S. Yao and C. An, **Integrated FeOOH nanospindles with conductive polymer layer for high-performance supercapacitors**, J. Alloys and Compound, DOI: 10.1016/j.jallcom.2017.09.002.
8. Q. Shou, J. Cheng , L. Zhang , B. J. Nelson, X. Zhang, **Synthesis and characterization of a nanocomposite of goethite nanorods and reduced graphene oxide for electrochemical capacitors**, Journal of Solid State Chemistry, 185 (2012) , pp. 191–197.
9. L. O'Neill, C. Johnston, P. S. Grant, **Enhancing the supercapacitor behaviour of novel Fe_3O_4/FeOOH nanowire hybrid electrodes in aqueous electrolytes,** Journal of Power Sources, 274 (2015), pp. 907-915.
10. M. Huang, Y. Zhang, F. Li, Z. Wang, A., N. Hu, Z. Wen, Q. Liu, **Merging of Kirkendall Growth and Ostwald Ripening: CuO@MnO_2 Core-shell Architectures for Asymmetric Supercapacitors,** 4 (2014), pp. 4518, DOI:10.1038/srep04518.
11. J. Chen, J. Xu, S. Zhou, N. Zhao, C.-P. Wong. **Amorphous nanostructured FeOOH and Co–Ni double hydroxides for high-performance aqueous asymmetric supercapacitors**, Nano Energy, 21 (2016), pp. 145-153.
12. Y. X. Zhang, X. D. Hao, Z. P. Diao, J. Li, Y. M. Guan, **One-pot controllable synthesis of flower-like $CoFe_2O_4$/FeOOH nanocomposites for high-performance supercapacitors** Materials Letters, 123 (2014), pp. 229–234.
13. Y. Wei, R. Ding, C. Zhang, B. Lv, Y. Wang, C. Chen, X. Wang, J. Xu, Y. Yang, Y. Li, **Facile synthesis of self-assembled ultrathin α-FeOOH nanorod/graphene oxide composites for supercapacitors**, Journal of Colloid and Interface Science, 504 (2017), pp. 593–602.